

Analysis of the GNSS Error Distribution for the Generation of a Cooperative Environment Model for Advanced Driver Assistance Systems

Florian Alexander Schiegg^{1,2}, Tobias Frye^{1,2} and Florian Wildschütte²

¹*Institute of Communications Technology, Leibniz University of Hannover, Appelstraße 9A, Hannover, Germany*

²*Robert Bosch GmbH, Corporate Research, Robert-Bosch-Strasse 200, Hildesheim, Germany*

Keywords: GNSS-Positioning, Localization Accuracy, V2x-Communication, Congestion Control.

Abstract: In the context of rising traffic automation, the generation of a reliable environmental model plays a key role. By sharing their information, vehicles and infrastructure are able to set up cooperative environmental models of considerably increased accuracy. The GNSS-based localization receives special attention in this regard, since it allows switching from vehicle relative coordinates to absolute and vice versa. While the focus of most related work lies on improving the mean of the GNSS fix, the work at hand analyses its error distribution. Field tests were performed on various scenarios and compared with simulations. Finally, a utility function is proposed, revealing the amount of information carried by every description parameter of the respective distribution.

1 INTRODUCTION

The ongoing trend towards automation on the streets has come along with the need for increasingly accurate environmental models. In this context vehicle to infrastructure (V2I) and vehicle to vehicle (V2V) communication have received growing interest in the past years. They allow to improve the environmental model obtained from the vehicles' own on-board sensors by fusing it with data from the incoming V2X-messages.

Sensor measurements, however, are faulty and every object's state is associated with a certain error distribution. Fusion algorithms, like the Kalman filter, heavily rely on an accurate estimation of these errors to weight the data of the different sensors. Also, the association of a measurement to a specific object within the environmental model is done based on the estimation of its associated error.

The GNSS localization receives special attention in the V2X context, since the information shared has to be transformed from the emitting vehicle's relative coordinates to absolute and later back to the receiving vehicle's coordinates. Hence, due to error propagation, all transmitted data is subject not only to the underlying sensors' intrinsic precision, but also to the absolute localization errors of both vehicles. An

exact estimation of the GNSS positioning error is thus of utmost importance.

In this work, different error estimations of the GNSS-based localization are compared. Based on these results, a utility function for the information content of every additional description parameter is set up, and the plausibility of the results is finally investigated by means of Monte Carlo simulations.

2 STATE OF THE ART

While there are a vast variety of proposed localization methods, the literature aimed at the estimation of its accuracy is considerably scarcer. Pullen, Walter, and Enge (2011) address the need for adapting existing integrity concepts from specific risk (e.g. aviation) to average risk applications (e.g. train and automotive). Since most receivers only write out specific sentences of the NMEA 183 standard defined by the National Marine Electronics Association (2008), a generic approach is needed to estimate the localizations error distribution (e.g., Cosmen-Schortmann et al., 2008; Mahdia et al., 2015). For its applicability in the automotive sector, the estimation has to be feasible in real time (e.g., Streiter et al., 2012 & 2013; Margaria & Faletti, 2014; Mahdia et al., 2015). It would further

be desirable to take into account shape-information about the error distribution comprised by the satellite constellation (e.g., Kaplan, 2005; Margaria and Faletti, 2014). This work attempts to cope with these issues simultaneously.

3 METHODOLOGY

This section describes the methods employed throughout this work. Section 3.1 briefly introduces the employed mathematical models and the evaluation of the results. The data collection is then described in section 3.2.

3.1 Theoretical Background

3.1.1 Horizontal Dilution of Precision

As mentioned previously, the constellation of the satellites used for the localization contains information concerning the shape of the positioning-error. The error vector can be written as (Kaplan, 2005):

$$d\mathbf{x} = \mathbf{H}^{-1}d\boldsymbol{\rho} \quad (1)$$

where $d\boldsymbol{\rho}$ represents the pseudorange error and

$$\mathbf{H} = \begin{bmatrix} u_{x,1} & u_{y,1} & u_{z,1} & 1 \\ u_{x,2} & u_{y,2} & u_{z,2} & 1 \\ \vdots & \vdots & \vdots & \vdots \\ u_{x,k} & u_{y,k} & u_{z,k} & 1 \end{bmatrix} \quad (2)$$

is a matrix composed of the satellite positions relative to the GNSS receiver

$$\begin{pmatrix} u_{x,k} \\ u_{y,k} \\ u_{z,k} \end{pmatrix} = \begin{pmatrix} \sin(Az_k)\cos(El_k) \\ \cos(Az_k)\cos(El_k) \\ \sin(El_k) \end{pmatrix} \quad (3)$$

Az_k and El_k are the azimuth and elevation of the k -th satellite respectively. The covariance can then be obtained from the expected value of the error vector:

$$cov(d\mathbf{x}) = E[d\mathbf{x}d\mathbf{x}^T] \quad (4)$$

By introducing Eq. 1 into Eq. 4 one then obtains

$$\begin{aligned} cov(d\mathbf{x}) &= E(\mathbf{H}^{-1}d\boldsymbol{\rho}d\boldsymbol{\rho}^T\mathbf{H}^{-T}) \\ &= \mathbf{H}^{-1}\mathbf{H}^{-T}cov(d\boldsymbol{\rho}) = (\mathbf{H}^T\mathbf{H})^{-1}\sigma_{URE}^2 \end{aligned} \quad (5)$$

In the second step $cov(d\boldsymbol{\rho}) = \sigma_{URE}^2$ was assumed to be constant. This approach assumes a multivariate Gaussian distribution of the error vectors and is often

utilized in literature for its good results and simplicity. σ_{URE} is the so-called user equivalent range error that describes the error contributions from the ionosphere, troposphere, multipath propagation, receiver noise, clock and ephemeris, and usually takes values between 0.5m and 10m depending on the quality indicator of the used receiver. A deeper treatment is offered by Kaplan (2005). While the user equivalent range error is a mere factor, the matrix

$$\mathbf{D} = (\mathbf{H}^T\mathbf{H})^{-1} = \begin{bmatrix} D_{11} & D_{12} & D_{13} & D_{14} \\ D_{21} & D_{22} & D_{23} & D_{24} \\ D_{31} & D_{32} & D_{33} & D_{34} \\ D_{41} & D_{42} & D_{43} & D_{44} \end{bmatrix} \quad (6)$$

contains the information about the errors shape. It is called the dilution of precision (DOP) matrix.

3.1.2 Error Morphologies

The upper left 2x2 part of the DOP matrix contains all relevant information about the 2D localization error. For symmetry reasons, it consists of only three independent parameters. By simple math it is possible to obtain the characteristic ellipse-shaped confidence intervals of the bivariate-Gauss-distribution (red area in Fig 1).

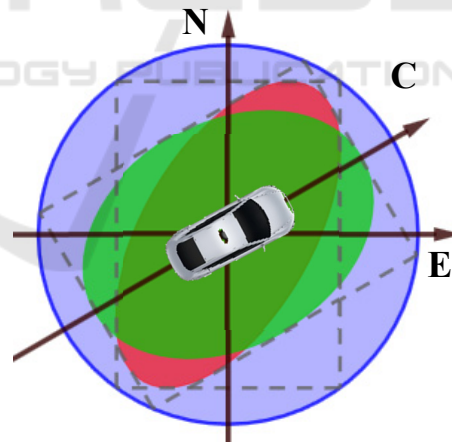


Figure 1: Error estimation morphologies.

In some cases, the system can be satisfactorily described by two parameters. For instance, for some applications only the error parallel and perpendicular to the driving direction \mathbf{C} is of interest. This is usually the case when the GNSS data stays on-board and is not transmitted to the surrounding V2X-capable traffic objects. The DOP matrix is then transformed to the ego-coordinate system of the GNSS receiver and the resulting correlation terms are set to zero,

resulting in an ellipse aligned with the driving direction (green area in Fig. 1).

For terrestrial applications, often only one parameter, the so-called horizontal dilution of precision (HDOP) is considered (Betz, 2016). It can be computed as

$$HDOP = \sqrt{D_{11} + D_{22}} \quad (7)$$

Multiplied by the UERE, it gives an estimation of the radius of a circle-shaped error distribution (blue area in Fig. 1).

For simplicity's sake the introduced error distributions will further be referred to by the number of their description parameters (e.g. the circle would be called the 1 parameter ellipse (1PE)).

3.1.3 Evaluation

To obtain a sufficiently accurate environmental model it is crucial to know which error estimate is most suitable for each scenario. Further, it would be desirable to determine how much information is carried by each supplementary description parameter to provide some sort of utility function and herewith allow a case specific evaluation of the parameters to be transmitted.

In order to make the error distributions comparable it has to be made sure they all represent the same confidence interval. For three main reasons the empirical UEREs supplied by literature are insufficient in this regard: (i) The UEREs vary significantly between different sources, (ii) the elimination of the correlation terms and the resulting diverging areas of the different error estimations imply modified confidence intervals, and (iii) the localization error is sensitively dependent on the algorithms and hardware employed by each GNSS receiver.

Hence, the UERE must be adjusted for each distribution in a way that it correctly predicts an equal number of measurements. This done, the estimations can finally be compared based on the proportion of estimations they do best and the average area necessary to meet the described normalization requirements. The latter is particularly important since it yields the accuracy of a model in form of its resolution.

3.1.4 Monte Carlo Simulations

Assuming the error distribution is completely random and thus uncorrelated to the inclination angle of the 3PE, then statistically 50% of the measurements would lie up to 45° away from its major axis. In other

words, in half of the cases the ellipse would describe the error more precisely than the circle. On the other side, should the error distribution be perfectly described by the covariance matrix, then the amount of situations the 3PE predicts the error in a better way depends on its deformation. Fig. 2 shows an ellipse with deformations a) $\epsilon = 1.3$ and b) $\epsilon = 2.0$ representing a random confidence interval of the error distribution. It is superposed by a circle of the same area and thus, resolution. Measurements located on the illustrated straight lines through the intersections of circle and ellipse will thus be equally well predicted by both geometries with equal resolution. On these lines, the Mahalanobis-distances of both models would also be alike. It can be noted that the Mahalanobis-distance of a 3PE is smaller in the red area than that of the 1PE and vice-versa for the blue area.

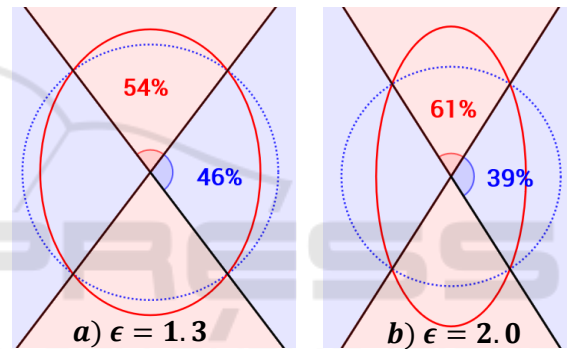


Figure 2: Region where the 1PE (blue) and the 3PE (red) require lower UEREs to describe the error for an ellipse deformation of a) $\epsilon = 1.3$ and b) $\epsilon = 2.0$ respectively.

Similar thoughts apply for the expected relative resolution of the estimations and the 2PE. Making use of Monte Carlo simulations it is hence possible to numerically predict how well the investigated models should describe the actual data, assuming either a fully random distribution or one perfectly described by the DOP matrix. Comparing these theoretical values with the experimental results makes it possible to draw conclusions on the nature of the real error distribution.

3.2 Experimental Setup

Experiments were carried out to investigate the performance of the proposed error estimates. To this purpose a test vehicle equipped with an ADMA-g Pro as ground truth reference was used to collect data on over 100 km in different scenarios (urban, countryside and highway). The measurements were

performed with two different test receivers, namely an Adafruit Ultimate GPS (MTK3339 chipset) and a u-blox EVK-M8T (NEO/LEA-M8T chipset). For further diversification SBAS was activated only on the former. All in all, over 45000 localizations were carried out (Table 1).

Table 1: Description of the investigated tracks.

Track	Scenario	Receiver	Distance
1	Mixed	Adafruit	10.9 km
2	Mixed	Adafruit	5.2 km
3	Highway	Adafruit	27.2 km
4	Mixed	Adafruit	6.1 km
5	Highway	Adafruit	39.1 km
6	Country Side	u-blox	12.1 km
7	Mixed	u-blox	9.2 km
8	Urban	u-blox	3.3 km

4 RESULTS AND DISCUSSION

4.1 Data Characterization

A characterization of the measurements for both test receivers and in distinct scenarios is provided in table 2. Interestingly the average horizontal error of the u-blox presented significantly lower values than the Adafruit with activated SBAS. Even in strongly screened areas it was able to detect a larger amounts of satellites, resulting in only moderately deformed ellipses ($\epsilon \sim 1.26$).

It is worth noticing that the Adafruit lost connection on a segment of the highway, yielding either no fix or extremely high errors (Fig. 4b). Since the overall average is of interest and this situation is not uncommon, these points were not filtered out.

Further, the used test receivers employ internal correction algorithms that lead to inertial effects on

the vertices of the trajectories, as can be seen in detail in figure 3. The effect is also well visible in a larger scale in figure 4a, where the best fitting error estimation changes briefly after most of the vertices. Since the vast majority of receivers employ internal correction algorithms and their influence on the results cancel out for sufficiently large amounts of data, the fixes were taken without further modifications.

4.2 Normalization

In a first step, the exact UERE was determined for each error estimation (Fig. 3). This means that the diameter of the geometries was chosen in a way that the measured fix lies right on its border.

The lower row of figure 4 shows the error estimate of highest resolution for every measurement. The only best fitting estimate was amplified by a factor of 10 for better visualization. As can be noted, in all scenarios the 3PE described the real error more accurately (lower area) than 1PE and 2PE. It should be kept in mind that only the portion of fixes best described by each geometry is of interest in this case, and not the area. Thus the colours may be a bit misleading at first sight.

The amount of fixes where the 3PE presented a lower area than the 2PE ranged from 52% in urban areas to 78% on the highway. The obtained values are shown on table 2.

However, since in practice the estimation has to be made in real time, a fix UERE has to be determined in advance. Fig. 5a and 5b show the number of measurements correctly predicted by each distribution as a function of the chosen UERE for the Adafruit and the u-blox respectively. As can be seen, the commonly used $UERE_{95\%}$ ranging from 5.0m to 7.1m (Betz et al., 2016; Kaplan, 2005) would contain only 70-86% of the Adafruit's but 100% of the

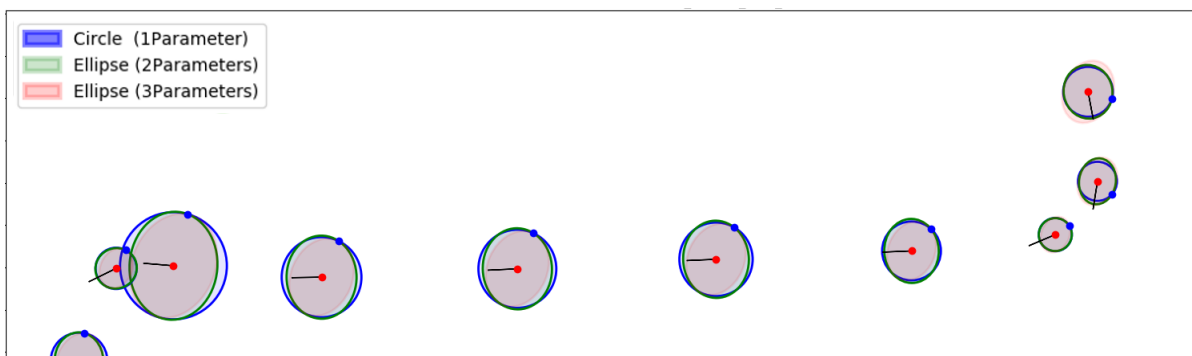


Figure 3: A posteriori calculated exact UEREs for given reference (red) and measurement (blue). The arrows point into the driving direction.

u-blox's measurements, confirming the necessity of its readjustment to ensure comparability.

It is worth noticing that even though different scenarios were analysed with each receiver, the cumulative error distributions converge in the same order for both (descending: 3PE, 2PE and 1PE).

4.3 Estimations Accuracies

Once the error estimations are normed to correctly predict equal numbers of measurements, they can be compared based on their resolution. As mentioned before, the resolution of an estimation is proportional to the inverse of its area. Table 2 summarizes the mean areas relative to the one of the 3PE at a confidence interval of 95% for the different scenarios. As could be expected from the previous results, both the 1PE and the 2PE require larger confidence intervals than the 3PE in three of the four investigated scenarios. Only in urban areas the 1PE seems to be

more accurate. However, by observing Fig. 6b the large oscillations stand out. It shows the areas of each distribution relative to that of the 3PE as a function of the confidence interval estimated with the determined fix UEREs. The oscillations are attributed to the size of the analysed sample (as a reference, for the Monte Carlo simulations to converge over 100 mio., simulated localizations were necessary). However, despite these oscillations the considerably lower relative performance of the 3PE is clearly visible. Thus, in areas with higher building density the DOP-matrix seems to lose validity. This effect may be explained by multipath propagation on the surrounding buildings, distorting the DOP matrix and leading to a more random distribution.

When comparing Fig 6a and 6b, a second effect can also be appreciated. Better receivers consider more satellites for their calculations, reducing the deformation of the ellipses, making them more similar to circles and reducing the impact of additional description parameters.

Table 2: Characterization of the collected data. In brackets the theoretical values obtained from Monte Carlo simulations.

Scenario	Mixed	Highway	Urban	Rural
GNSS Receiver	Adafruit	Adafruit	u-blox	u-blox
Absolute Error [m]	2.82 ± 1.70	5.19 ± 8.41	1.59 ± 0.65	0.91 ± 0.18
Deformation $\varepsilon = b/a$	1.37 ± 0.11	1.36 ± 0.24	1.26 ± 0.12	1.15 ± 0.09
$A_{3PE} < A_{1PE}$ (exact UERE)	0.67 (0.56)	0.78 (0.55)	0.52 (0.54)	0.66 (0.52)
Rel. Area A_{1PE}/A_{3PE} [95%]	1.26 (1.06)	1.21 (1.06)	0.96 (1.04)	1.09 (1.02)
Rel. Area A_{2PE}/A_{3PE} [95%]	1.17 (1.04)	1.04 (1.04)	1.00 (1.03)	1.06 (1.01)

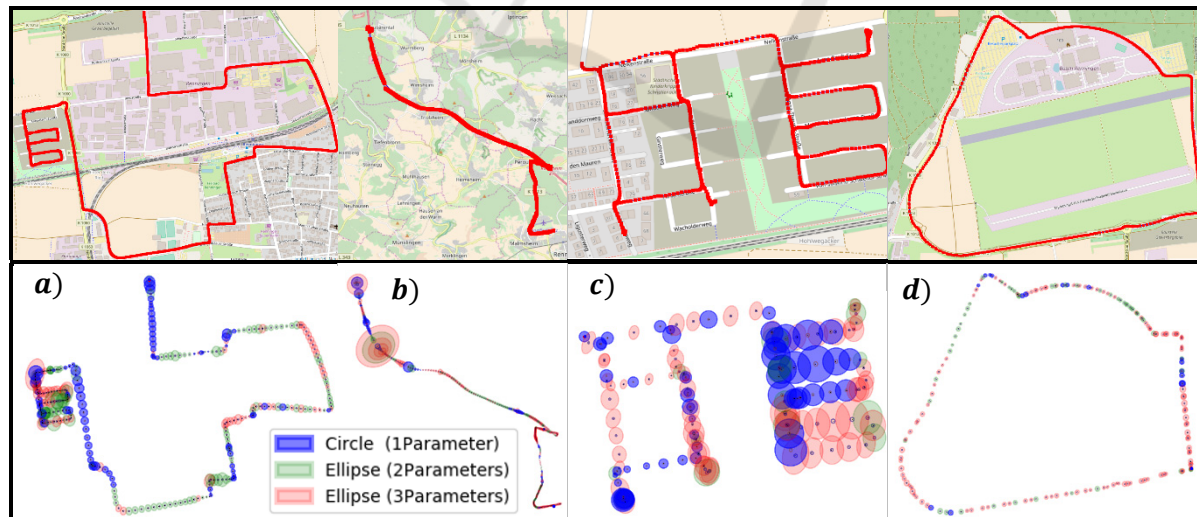


Figure 4: Selection of tracks for the different scenarios (upper row) and best describing error geometry (lower row) for a-posteriori computed exact UEREs (augmented by a factor of 10 for a better visualization).

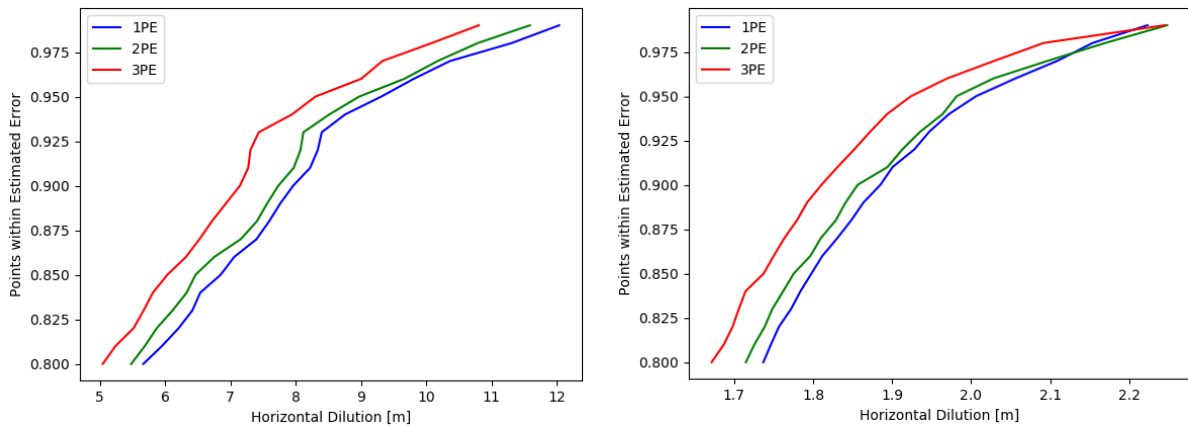


Figure 5: Cumulative error distributions of a) the Adafruit and b) the u-blox.

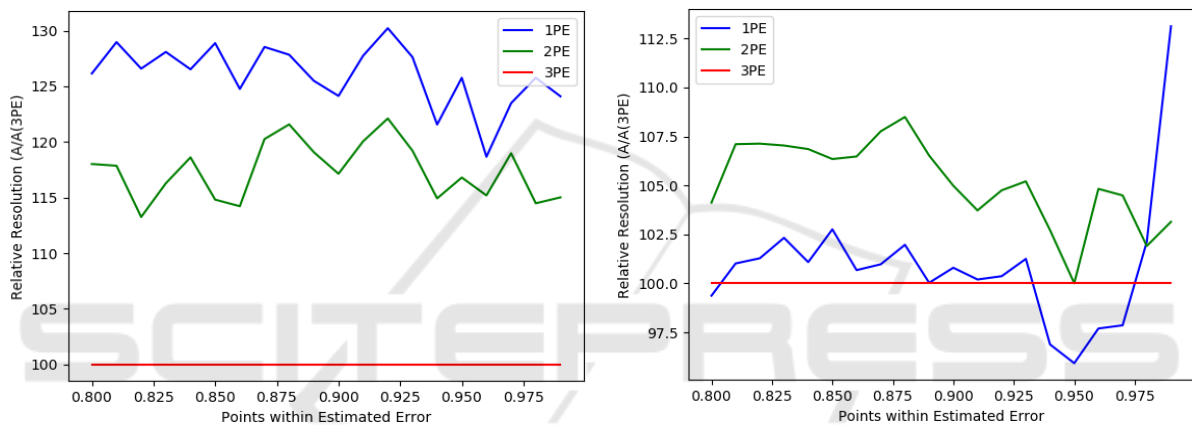


Figure 6: Relative mean area of the estimated confidence intervals, a) Adafruit, mixed and b) u-blox, urban.

With the obtained results it is then possible to partially construct a utility function to estimate the value of every additional parameter, depending on the scenario. In strongly shaded regions multipath randomly scatters the measured fixes of both receivers, significantly reducing the validity of the 3PE-model. However, in mainly open surroundings the 2PE was found to be in average 7% (2%) and the 3PE even up to 25% (8%) more accurate than the 1PE for the Adafruit (u-blox). which is a fairly large increase. In the ADAS-context an increase of this magnitude in accuracy presents a considerable improvement. Three key systems of highly automated vehicles profit from a more precise estimation of the localization error: (i) Association: To construct the environmental model for the ADAS-system to base its decisions on the objects detected by different sensors have to be associated. In the case of a cooperative environmental model, also the objects transmitted via V2X-communication have to be associated with those of the local environmental model. A precise knowledge of the data's accuracy is

essential. (ii) Sensor fusion: The data of an object provided by different sensors is then fused, weighted by the estimated accuracies. A better estimation of the GNSS localization error thus leads to a better overall localization after the data is fused with that of other sensors. (iii) V2X-communication: On-board sensors employ a relative coordinate system. To share data with other V2X-cappable vehicles, this data has thus to be transformed to absolute coordinates in the sending vehicle by means of its GNSS-fix and its accuracy. The receiving vehicle then has to transform it back to its own coordinate system, making use again of its absolute position and associated error estimation. A bad GNSS-error estimation will thus have a large negative impact on the transmitted sensor data.

This in mind, the performance increase provided by the 3PE with respect to the 1PE is thus considerable. However, it should be noted that the obtained values have to be taken with the appropriate caution. As the results showed, the utility function is

receiver specific and depends significantly on its quality.

4.4 Comparison with Simulations

Comparing these observations with the theoretical values determined by Monte Carlo simulations (listed in brackets in table 2) shows that in urban areas the real error distribution lies somewhere between that of a fully random distribution (ratio 50%) and that of the covariance matrix (ratio 54%).

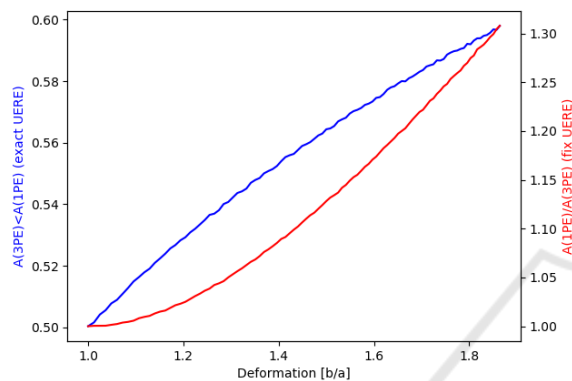


Figure 7: Dependence of the predictions performances on the distributions deformation (Monte Carlo simulations).

All other scenarios lie well above the theoretical value, proving that the covariance matrix is not only strongly correlated to the real error distribution in open sky areas, but also that higher axis ratios would describe it better with the same inclination angles, hinting systematic errors. Since this behaviour occurred equally for varying experimental conditions (e.g. speed, driving direction, satellite constellations, daytime, etc.) it can most probably be traced back to the receivers themselves. Many receivers rely on the weighted least squares method, which weights the used satellites independently. In single-frequency SPS receivers the pseudorange error measurements, dominated by ionospheric effects, can be approximated by the satellites' elevations (Kaplan, 2005, 332). This results in higher deformations of the error distributions. The same conclusions apply to the relative resolution of the analysed error estimations.

5 CONCLUSION

The main purpose of this work was to compare different error distributions of the GNSS localization derived from the satellite constellation. Field tests were performed in characteristic scenarios, at varying

conditions, daytimes, and test receivers. It could be shown that while shadowing has a positive effect on the distributions' eccentricity and thus on the 3PE relative accuracy, multipath propagation leads to the opposite result. The latter could be attributed to the distortion of the DOP matrix due to satellites erroneously taken into account. In open sky areas however, the 3PE estimation proved to perform considerably better than the simplified error distributions. Furthermore, the magnitude of this effect seemed to be correlated to the used test receiver. Cheaper receivers incorporate fewer satellites into their fixes, yielding more deformed error distributions. The gain of accuracy per transmitted parameter is thus notably higher than in expensive super accurate receivers. Simulations supported the experimental results; nevertheless, further research is highly encouraged.

REFERENCES

- Betz John W., 2016. *Engineering satellite based navigation and timing: Global Navigation Satellite Systems, Signals, and Receivers*. Wiley-IEEE Press.
- Cosmen-Schortmann, J., Azaola-Sáenz, M., Martínez-Olagüe, M., & Toledo-López, M., 2008. Integrity in Urban and Road Environments and its use in Liability Applications. *IEEE/ION Position, Location and Navigation Symposium*.
- Kaplan Elliott D., 2005, *Understanding GPS: Principles and Applications*. Artech House Publishers, London, 2nd edition.
- Margaria Davide and Faletti Emanuela, 2014. A novel local integrity concept for GNSS receivers in urban vehicular contexts. *IEEE/ION Position, Location and Navigation Symposium*.
- National Marine Electronics Association (NMEA), 2008, NMEA 0183 Standard, viewed 1 December 2017, <http://www.nmea.org/>
- Pullen Sam, Walter Todd, and Enge Per, 2011. SBAS and GBAS Integrity for Non-Aviation Users: Moving Away from Specific Risk. *International Technical Meeting of the Satellite Division of the Institute of Navigation*.
- Streiter Robin, Bauer Sven, Bauer Stefan, and Wanielik Gerd, 2013. GNSS Correction Services for ITS Applications: A performance Analysis of EGNOS and IGS. *IEEE Intelligent Transportation Systems*.
- Streiter Robin, Bauer Sven, Bauer Stefan, and Wanielik Gerd, 2012. GNSS Multi Receiver Fusion and Low Cost DGPS for Cooperative ITS and V2X Applications. *9th ITS Europe Congress*.
- Tahsin Mahdia, Sultana Sunjida, Reza Tasmia, and Hossam-E-Haider Md, 2015. Analysis of DOP and its Preciseness in GNSS Position Estimation. *Electrical Engineering and Information Communication Technology*.